ACS Photonics

Article

Cite This: ACS Photonics 2018, 5, 4371−4377

pubs.acs.org/journal/apchd5

Optomechanical Manipulation with Hyperbolic Metasurfaces

Aliaksandra Ivinskaya,*[,†] Natalia Kostina,[†] Alexey Proskurin,[†] Mihail I. Petrov,[†] Andrey A. Bogdanov,[†,▽] Sergey Sukhov,[‡,§] Alexey V. Krasavin,[∥] Alina Karabchevsky,[⊥,#] Alexander S. Shalin,[†,○] and Pavel Ginzburg[□,△]

[†]Department of Nanophotonics and Metamaterials, ITMO University, Birzhevaja line, 14, 199034 St. Petersburg, Russia

[‡]CREOL, The College of Optics and Photonics, University of Central Florida, Orlando, Florida 32816, United States

[§]Kotel'nikov Institute of Radio Engineering and Electronics of Russian Academy of Sciences (Ulyanovsk branch), 48/2 Goncharov Str., 432071 Ulyanovsk, Russia

[∥]Department of Physics, King's College London, Strand, London WC2R 2LS, United Kingdom

[⊥]Electrooptical Engineering Unit, Ben-Gurion University, Beer-Sheva, 8410501, Israel

[#]Ilse Katz Institute for Nanoscale Science and Technology, Ben-Gurion University, Beer-Sheva, 8410501, Israel

[○]Ulyanovsk State University, Lev Tolstoy Street 42, 432017 Ulyanovsk, Russia

[□]School of Electrical Engineering, Tel Aviv University, Ramat Aviv, Tel Aviv 69978, Israel

[△]Light−Matter Interaction Centre, Tel Aviv University, Tel Aviv, 69978, Israel

[▽]Ioffe Institute, St. Petersburg 194021, Russia

Supporting Information

ABSTRACT: Auxiliary nanostructures introduce additional flexibility into optomechanical manipulation schemes. Metamaterials and metasurfaces capable to control electromagnetic interactions at the near-field regions are especially beneficial for achieving improved spatial localization of particles, reducing laser powers required for trapping, and for tailoring directivity of optical forces. Here, optical forces acting on small particles situated next to anisotropic substrates, are investigated. A special class of hyperbolic metasurfaces is considered in details and is shown to be beneficial for achieving strong optical pulling forces in a broad spectral range. Spectral decomposition of Green's functions enables identifying contributions of different interaction channels and underlines the importance of the hyperbolic dispersion regime, which plays the key role in optomechanical interactions. Homogenized model of the hyperbolic metasurface is compared to its metal-dielectric multilayer realizations and is shown to predict the optomechanical behavior under certain conditions related to composition of the top layer of the structure and its periodicity. Optomechanical metasurfaces open a venue for future fundamental investigations and a range of practical applications, where accurate control over mechanical motion of small objects is required.

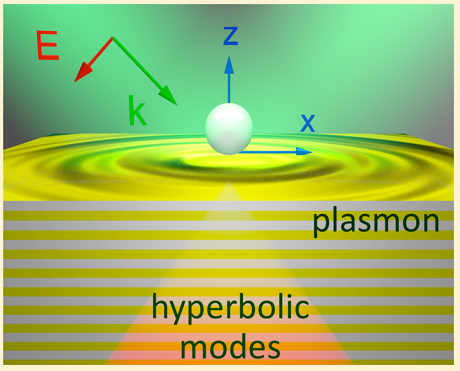

KEYWORDS: *optical pulling forces, optical tweezers, hyperbolic dispersion, multilayer, surface plasmon, tractor beam, anisotropic substrate, nanoparticle*

Control over mechanical motion of small particles with laser beams opened a venue for many fundamental investigations and practical applications.[1−3] Optical tweezers became one of the most frequently used tools in biophysical research, since they enable measuring dynamics of processes, control, and monitor forces on pico-Newton level; for example, see refs 4 and 5.

Classical optical tweezers, including the extension of the concept to holographic multitrap configurations,[6] are based on diffractive optical elements, and can provide trapping stiffness at the expense of an increased overall optical power. This limitation also applies to trapping with structured and superoscilatory beams (e.g., see ref 7). A promising solution for achieving improved localization and the highest possible stiffness within the trap is to introduce auxiliary nanophotonic or plasmonic structures that enable operation with nano-confined near fields. Plasmonic tweezers, for example, utilize localized resonances of noble metal nanoantennas and provide significant improvement in trap stiffness and spatial localization of trapped objects.[8] Optical manipulation with other auxiliary tools, for example, endoscopic techniques,[9] nanoapertures,[10] nanoplate mirrors,[11] and integrated photonic devices[12,1314] was also demonstrated. A special attention was paid to particles trapping next to surfaces, since a typical experimental layout of a fluid cell may include substrates of different kinds, for

Received: June 8, 2018
Published: October 17, 2018

DOI: 10.1021/acsphotonics.8b00775
ACS Photonics 2018, 5, 4371−4377

example, see refs 15 and 16 and others. Furthermore, controllable transport over surfaces enables a range of particles sorting applications.[13] Here, additional advantages of carefully designed surfaces in application to optomechanical manipulations will be investigated.

Introduction of additional flexibilities and degrees of freedom into manipulation schemes is required for achieving ultimate optomechanical control over particles' motion. Tractor beams are a vivid example of a peculiar phenomenon, where a particle moves against the global beam propagation direction toward a light source. Structured illumination was initially used for demonstration of this effect.[17−19] Remarkably, unstructured light, for example, plane wave, can result in pulling force on particles, situated above planar substrates.[20,21] Besides a special case, where beads were partially immersed into a media,[20] more practical configuration with a particle above the substrate was considered in ref 21 and pulling forces, owing to unidirectional excitation of surface plasmons, were predicted. Other recently reported phenomena of the optical forces, tailored with planar surfaces, include the force enhancement with Bloch modes.[22,23] An extended review on optical forces acting on a particle above a substrate is given in the Supporting Information, A.

Another approach to tailoring optomechanical interactions is to utilize the concept of metamaterials, which allows achieving control over propagation of light via subwavelength structuring of unit cells.[24] A special class of metamaterials is a hyperbolic medium,[25] which enhances the density of electromagnetic states and, as the result, enables controlling efficiency of scattering channels. Hyperbolic metamaterials, based on vertically aligned metal nanorods, were assessed as a platform for flexible optomechanical manipulation.[26,27] While a set of peculiar effects, including tractor beams, were predicted by employing homogenization approach,[27] consideration of near-field interactions within actual unit cells of the nanorod arrays require more detailed numerical analysis.[26] From a practical standpoint, optomechanical manipulation inside metamaterials may face additional challenges and undesirable constraints can emerge. On the other hand, metasurfaces (e.g.[28−30]) (in particular, hyperbolic) can share several advantages: delivering high density of electromagnetic states for tailoring scattering properties and providing direct physical access to manipulated objects (here they are located above the structure and not inside). Hyperbolic metasurfaces have already demonstrated superior characteristics in controlling surfaces waves and scattering, for example, see refs 31 and 32. Here, optomechanical interactions over hyperbolic metasurfaces will be analyzed and a set of new effects will be predicted. In particular, tailoring electromagnetic interactions with a particle by opening high density of states scattering channels will be shown to deliver puling forces in a broad spectral range owing to the hyperbolic nature of wave dispersion in the metamaterial substrate. This effect also makes the distinctive differences between this new approach to previously reported investigations (e.g., ref 21).

The proposed configuration, subject to the subsequent analysis, is depicted in Figure 1. A small dielectric bead is situated in a close proximity of layered metal-dielectric periodic substrate, which supports hyperbolic regime of dispersion of bulk modes. The structure is illuminated with a plane wave, which excites both surface plasmon and volumetric hyperbolic waves, owing to the scattering from the particle. The interplay between resonant and nonresonant contributions of different types of electromagnetic modes gives rise to strong pulling forces, which will be analyzed hereafter. Green's function formalism enables identifying contributions of different scattering channels to the overall optical force and, as a result, to develop clear design rules for tailoring optomechanical interactions.

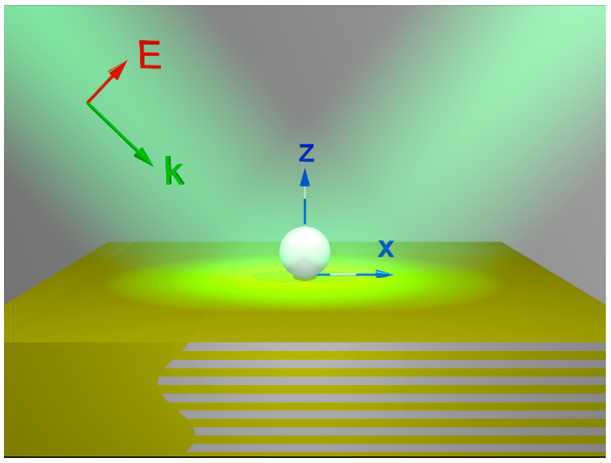

Figure 1. Optomechanically manipulated subwavelength dielectric particle next to anisotropic (hyperbolic) metasurface, illuminated with an obliquely incident plane wave. The origin of Cartesian coordinates is the point at the substrate−air interface below the geometric center of the particle.

The manuscript is organized as follows: general Green's function formalism in application to optical forces will be revised first and then applied to the case of the homogeneous hyperbolic metasurface. Conditions for achieving optical pulling forces will be derived and contributions of surface and volumetric waves will be identified. Analysis of a realistic layered structure will be performed and additional peculiar optomechanical effects will be discussed. Details of mathematical analysis and several optimization routines appear in the Supporting Information.

DIPOLE PARTICLE OVER ANISOTROPIC SUBSTRATE: GENERAL FORMALISM

Optical forces, acting on a small subwavelength particle, obeying dipolar approximation, can be expressed by[33] $F_j = \frac{1}{2}\mathrm{Re}(\alpha \mathbf{E}^{\mathrm{tot}} \cdot \partial_j \mathbf{E}^{\mathrm{tot}*})$, where $\mathbf{E}^{\mathrm{tot}}$ is a local field at the particle location, α is particle's complex polarizability taking into account radiation reaction, and subscript indexes stay for directions in the Cartesian coordinate system.[34] If a particle is situated next to a photonic structure, self-consistent electromagnetic field contains rescattering contributions between all the constitutive elements. In the case of a small particle next to a flat surface, transversal optical force can be calculated self-consistently via[21]

$$F_x = \frac{1}{2}\mathrm{Re}(\alpha \mathbf{E}^{\mathrm{tot}} \cdot \partial_x \mathbf{E}^{0*}) + |\alpha|^2 \omega^2 \mu_0 \mu_1 \mathrm{Im}(E_x^{\mathrm{tot}} E_z^{\mathrm{tot}*}) \mathrm{Im}(\partial_x G_{xz}) \quad (1)$$

where G_{xz} is a component of the Green's function tensor $\overleftrightarrow{\mathbf{G}}$ of a dipolar scatterer above a substrate, $\mathbf{E}^0$ is the electrical field of a wave incident and reflected from the substrate (calculated without a particle), and μ_0 and μ_1 (=1 in subsequent analysis) are permeabilities of vacuum and upper half-space. Green's function appears in both expressions for the total field $\mathbf{E}^{\mathrm{tot}}$ and the force $\mathbf{F}$(see Supporting Information, B for details). Both summands in eq 1 influence transversal optical force F_x,

DOI: 10.1021/acsphotonics.8b00775
ACS Photonics 2018, 5, 4371−4377

however, for realistic materials the first term is positive and comparable with free-space force magnitude, while the second one might take large values, resulting from Green's function component ($\partial_x G_{xz}$) and excitation conditions, given by $\mathrm{Im}(E_x^{tot}E_z^{tot*})$. The product $\mathrm{Im}(E_x^{tot}E_z^{tot*})\mathrm{Im}(\partial_x G_{xz})$ with an appropriate sign might change the overall balance and result in an attracting force (see Supporting Information, C).

Green's function encapsulates the response from the auxiliary layered structure, which manifest itself via reflection coefficients r_s and r_p for s and p polarizations. Here, the whole set of the plane waves, including propagating and evanescent ones, should be taken into account. Evanescent components are generated by the particle, which are near-field coupled to the surface. In the case of a hyperbolic substrate, both surface and bulk waves can be supported (note that hyperbolic metamaterials convert evanescent fields into propagating ones owing to the peculiar law of dispersion). The excitation efficiency of different modes depends on density of states (DOS); in the case of surface plasmons it has strongly resonant behavior, while hyperbolic bulk modes have high DOS over a broad spectral range. Those properties enable separating different electromagnetic channels via the Fourier spectrum representation of the Green's function and, as a result, identify the main contributing mechanism for achieving strong opto-mechanical interactions.

It is worth noting that Green's functions in flat layer geometries (one among possible ways to construct an artificial hyperbolic metamaterial) has analytical expressions, allowing direct comparison between performances of homogenized media and its possible realization. From the applied standpoint, fabrication of nanometre thin layers is possible with atomic layer deposition techniques, for example, see refs 35−37, which makes the theoretically developed concept to be attractive from the experimental perspectives.

OPTICAL ATTRACTION, MEDIATED BY HYPERBOLIC SUBSTRATES

The impact of homogenized anisotropic substrates on optical forces will be studied next. Figure 2a,b shows transversal force F_x acting on a small dielectric particle above a uniaxial crystal as calculated with eq 1. The force map is built as a function of real parts of dielectric permittivities along the two main axes $\varepsilon_x = \varepsilon_x' + i\varepsilon_x''$ and $\varepsilon_z = \varepsilon_z' + i\varepsilon_z''$ of the crystal. Regions of positive and negative values of the force are displayed with gray and color legends, respectively. Each quadrant (marked on panel (a)) on the force map corresponds to a different regime of the substrate's dispersion. The first quadrant shows the normal elliptical regime of dispersion, which does not support any surface waves and high DOS volume waves. As a result, an attraction force cannot be achieved. The third quadrant, where both components of the tensor are negative, corresponds to the regime of surface plasmon modes, while the bulk substrate does not support any propagation of waves within its volume. In this case, a strong attraction can be achieved owing to the surface mode, as was previously demonstrated,[21] owing to unidirectional excitation of plasmons. Clear resonant plasmonic branch is seen on the force map. The width of the force resonance becomes wider with the increase of the material loss (panel (b)). Quadrants II and IV support the regime, when both surface plasmon and hyperbolic bulk modes can be supported. Remarkably, the main difference in the force behavior (no attraction at the forth quadrant) emerges owing to the orientation of the polarization of the incident field with respect to the negative component of permittivity tensor. This behavior can be retrieved by analyzing the balance between $\mathrm{Im}(\partial_x G_{xz})$ and $\mathrm{Im}(E_x E_z^*)$, see Supporting Information, Figure S1 and the corresponding discussion.

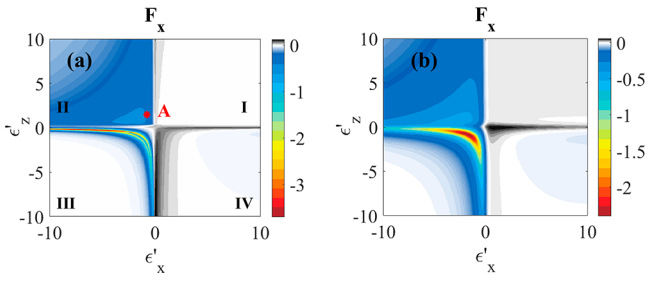

Figure 2. Color maps of optical forces (in fN mW^{-1} μm^2) acting on a particle (ε = 3, R = 15 nm, z = 15 nm) above an anisotropic material, as the function of real parts of the substrate tensor parameters ε_x',ε_z'. Material losses are set to (a) ε_x'',ε_z'' = 0.05, (b) ε_x'',ε_z'' = 0.3. Plane wave is incident at 35° in respect to the normal, λ = 450 nm. Balances between the force components at the regime, marked by point A, will be analyzed in Figure 3.

While the regime of the second quadrant supports the surface waves, a clear plasmonic branch in the force map is not observed. The balance between different contributions will be analyzed next; it is worth re-emphasizing that hyperbolic materials can support both surface and bulk waves. Volumetric waves with hyperbolic dispersion have nonresonant features, whereas existence of surface modes can be identified via observation of poles in the reflection coefficient. Those coefficients for the case of the uniaxial crystal with an optical axis, pointing perpendicular to the interface, are given by[38,39]

$$r_p = \frac{\varepsilon_x k_{1z} - \varepsilon_1 k_{2z}^p}{\varepsilon_x k_{1z} + \varepsilon_1 k_{2z}^p},\ k_{2z}^p = \left(\varepsilon_x k_0^2 - \frac{\varepsilon_x}{\varepsilon_z} k_\rho^2\right)^{0.5},\ k_{1z} = (\varepsilon_1 k_0^2 - k_\rho^2)^{0.5} \quad (2)$$

where k_0 is a wave vector of incident radiation in vacuum, ε_1 and $k_1 = \sqrt{\varepsilon_1} k_0$ are the permittivity and the wave vector in the upper half-space (air is considered hereafter) with components k_x, k_y, k_{1z}, and $k_\rho = (k_x^2 + k_y^2)^{0.5}$ is a transversal component of the wave vector. The branch of the square root solution in eq 2 should be chosen with imaginary part of k_{2z}^p (wave vector in the substrate) positively defined for a wave to decay away from the interface. At the same time, for idealized lossless hyperbolic materials, having different signs of ε_x',ε_z', component of the wave vector k_{2z}^p acquires real part for $k_\rho = k_{cr} \geq k_1$. It implies that at this condition evanescent waves scattered by the particle transform into propagating volume modes inside the hyperbolic substrate.[40] On the other hand, the pole in the reflection coefficient (eq 2) gives the dispersion of the surface plasmon propagating over an anisotropic substrate:

$$k_\rho^{pl} = k_0 \left(\frac{(\varepsilon_1 - \varepsilon_x)\varepsilon_1 \varepsilon_z}{\varepsilon_1^2 - \varepsilon_x \varepsilon_z}\right)^{0.5} \quad (3)$$

Surface plasmon resonance condition is fulfilled once the real part of the denominator of in eq 3 goes to zero.

In order to find the contributions of surface and volumetric waves to the pulling force, the integral representation of Green's function can be used. At the close proximity of a particle to the substrate ($z \ll \lambda$), several contributions to the derivative $\partial_x G_{xz}$ can be identified:

DOI: 10.1021/acsphotonics.8b00775
ACS Photonics 2018, 5, 4371−4377

$$\partial_x G_{xz} = \frac{1}{8\pi k_1^2}\int_0^\infty r_p k_\rho^3 e^{2ik_{1z}z}\mathrm{d}k_\rho = \frac{1}{8\pi k_1^2}$$
$$\left\{\int_0^{k_1} + \int_{k_1}^{k_{cr}} + \int_{k_{cr}}^{\infty}\right\} r_p k_\rho^3 e^{2ik_{1z}z}\mathrm{d}k_\rho = g^{pr} + g^{pl} + g^{hb} \quad (4)$$

This splitting of integral into g^{pr}, g^{pl}, and g^{hb} summands underlines the contribution of the free space propagating (in the air superstrate), plasmon, and hyperbolic modes. Linking those parts of the integral with the beforehand mentioned physical interpretation can be done under several approximations. First, the particle should be located in the close proximity of the substrate in order to excite both plasmon and volume modes efficiently. Second, the plasmonic mode should have a narrow pole in the reflection coefficient, which is perfectly satisfied in the case of the low loss hyperbolic material.

Three spectral intervals, underlined in eq 4, can be identified by observing the imaginary part of the reflection coefficient r_p, Figure 3a (s-wave reflects similar to pure metal case and r_s does not contribute to $\partial_x G_{xz}$). As it is shown by eq S8 in Supporting Information, A, $\mathrm{Im}(\partial_x G_{xz})$ is primarily defined by $\mathrm{Im}(r_p)$ and the proposed separation of different modes contributions to the optical force given by eq 4 and is justified.[40] In the hyperbolic regime, the reflection coefficient is virtually constant at larger k_ρ and using $r_p^\infty = r_p(k_\rho/k_1 \to \infty)$ for evaluation of g^{hb} (one of the summands in eq 4) is a rather good approximation. With $r_p^\infty = (\sqrt{\varepsilon_x\varepsilon_z} - \varepsilon_1)/(\sqrt{\varepsilon_x\varepsilon_z} + \varepsilon_1)$ the term g^{hb} can be analytically integrated to the simple form:

$$g^{hb,ap} = \frac{3r_p^\infty}{4\pi k_1^2 (2k_1 z)^4} \quad (5)$$

Note that the exact value of k_{cr} has only a minor contribution to the integration of $g^{hb,ap}$ as long as $k_{cr}z$ is small (this is the manifestation of the nonresonant nature of high DOS in homogeneous hyperbolic metamaterials). $g^{hb,ap}$ is symmetric with respect to $\varepsilon_x,\varepsilon_z$ as follows from the expression for r_p^∞. Figure 3b demonstrates the plot of the term $g^{hb,ap}$ together with actual value of $\partial_x G_{xz}$. Here either ε_x' or ε_z' is fixed to −0.5, while another component is varied and $\partial_x G_{xz}$ is evaluated. Note that $g^{hb,ap}$ has the same value if ε_x' and ε_z' interchange their roles, while $\partial_x G_{xz}$ demonstrates a slight difference in the real part. It is evident that $g^{hb,ap}$ strongly prevails the overall value of $\partial_x G_{xz}$ and all other contributions (see eq 4) can be neglected. As a result, pulling forces, observed in quadrant II (Figure 2), mainly arise due to volume hyperbolic modes. Finally, it is worth noting, that optical forces are not symmetric in respect with interchanging the roles of ε_x' and ε_z', since the polarization of the excitation and direction of propagation affects differently the value of $\mathrm{Im}(E_x^{tot}E_z^{tot*})$ (eq 1), see the Supporting Information, C.

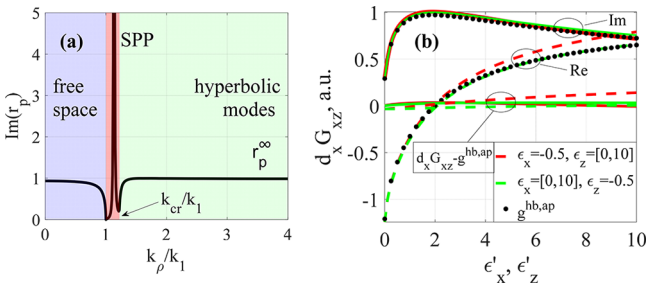

Figure 3. (a) Reflection coefficient for hyperbolic material as a function of transversal component of the wave vector k_ρ. The parameters of the system correspond to point A from Figure 2a with $\varepsilon_x' = -0.5$, $\varepsilon_z' = 1.1$, ε_x'', $\varepsilon_z'' = 0.01$. (b) Green's function derivative $\partial_x G_{xz}$ (both real and imaginary parts) above the anisotropic substrate at coordinate $z = 15$ nm. Two cases are plotted: $\varepsilon_x' = -0.5$, $\varepsilon_z' \in [0,10]$ (red lines) and, vice versa, $\varepsilon_x' \in [0,10]$, $\varepsilon_z' = -0.5$ (green lines). Black dots correspond to approximate value $g^{hb,ap}$ (eq 5). Imaginary part of the permittivity was taken to be $\varepsilon_x'',\varepsilon_z'' = 0.05$.

MULTILAYER SUBSTRATES FOR NEGATIVE TRANSVERSAL FORCE

Metal-dielectric multilayers are one among probable realizations of hyperbolic metamaterials.[36] The goal of the subsequent studies is to compare performance of realistic composites with their homogenized counterparts, investigated in the previous section. Silver layers interchanging with a transparent dielectric (e.g., made of porous polymer, refractive index $n = 1.05$) will be studied next. Effective material properties can be attributed to those composites if the periodicity of the structure and thicknesses of layers are significantly smaller than the wavelength. In this case, the effective dielectric tensor is given by $\varepsilon_x = \varepsilon_1 f_1 + \varepsilon_2(1 - f_1)$, $\varepsilon_z = (f_1\varepsilon_1^{-1} + (1 - f_1)\varepsilon_2^{-1})^{-1}$, where $\varepsilon_1,\varepsilon_2$ are permittivities of metal

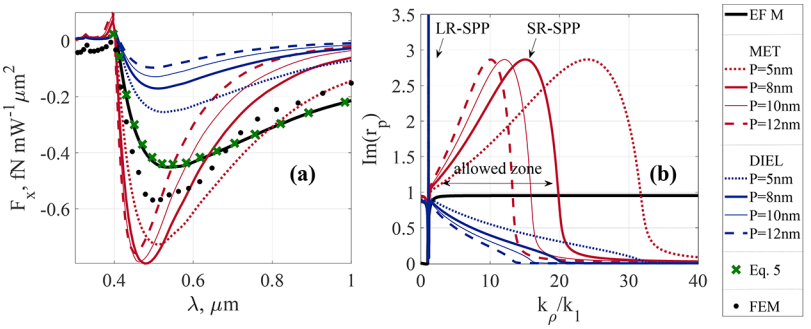

Figure 4. (a) Transversal force F_x acting on a particle, as a function of the wavelength. (b) Imaginary part of the reflection coefficient for semi-infinite Ag-polymer multilayer composite as the function of the transverssal component of the wave vector. Red (blue) lines correspond to the case, when the top layer, interfacing the air, is metal (dielectric). Black line is obtained within the effective medium approach; green crosses correspond to approximation given by eq 5; black dots correspond to numerical simulation of a particle a distance $z = 16.5$ nm above anisotropic substrate. A set of multilayer periods P is specified in the legend. Other parameters are $R = 15$ nm, $\varepsilon = 3$, $z = 15$ nm, and $f_1 = 0.2$, and the structure is illuminated by a plane wave incident at 35°.

DOI: 10.1021/acsphotonics.8b00775
ACS Photonics 2018, 5, 4371−4377

and dielectric, $f_1 = d/$ is filling fraction of metal of thickness d in the unit cell of period .[40] While this homogenization approach works extremely well in the case of a small dielectric contrast between the constitutive materials, it might face several limitations, if plasmonic layers are alternating with positive epsilon dielectrics.[35] Spatial dispersion effects,[41] fast-decaying evanescent waves next to metamaterial−air interfaces,[42] local near-field corrections,[40] and others should be taken into account,[26,27] depending on a specific phenomenon under consideration. Hereafter, homogenization approach to layered metamaterials is assessed in application to optical forces (see also Supporting Information, D).

The exact reflection coefficients for semi-infinite multilayer are obtained according to the approach developed in.[40] The material composition of the first layer (either metal or dielectric) has a crucial impact on the pulling force. This effect is solely related to the realization of the metamaterial and, of course, cannot be observed in the studies of the homogenized substrate. Those three different scenarios, first metal layer, first dielectric layer, and homogeneous substrate are considered hereafter. Figure 4a demonstrates the value of the pulling force (negative value = pulling), as the function of wavelength of the incident radiation (the silver filling factor is fixed at $f_1 = 0.2$). Corresponding homogenized substrate has effective parameters, corresponding to point A in Figure 2a. Results of a finite-element method (FEM) simulation, performed with Comsol Multiphysics, are shown with black dots. The values of the force for the homogenized case typically lie in between those of multilayer realizations with either dielectric (blue lines) or metal (red lines) top layer. If metal is set as an outer layer, maximum force amplification is achieved. At the longer wavelengths (infrared) regimes of metal or dielectric top layer can give an order of magnitude difference in force values (see Supporting Information, Figure S3). As it is expected, multilayers with smaller period (P in the captions; closely resembling the homogenized description) have broadband spectra, while larger periods give sharper features and a slight blue shift of the resonant frequency. The homogenized model perfectly predicts the behavior of the multilayer composite, if the period of the latter is as small as 0.5−1 nm, which seems to be unrealistic with the current fabrication technologies. Furthermore, in order to underline features, provided by multilayers versus homogeneous substrate, the particle was chosen to touch the outer layer of the composite. As the distance to substrate is increased, the discrepancies between two approaches become minor.[43] In order to verify the validity of the developed theoretical approach, full wave finite element numerical simulation was performed (black dots). A 30 nm particle above homogeneous substrate was investigated. Qualitatively good agreement between the numerical and analytical results was achieved. The discrepancies are attributed to the finite volume of the particle, which was fully accounted in the case of FEM simulation and was considered in the dipolar approximation in the analytical theory.

Additional optimization over the layers' parameters in order to achieve maximal pulling force can be performed and is discussed in the Supporting Information, D and E. It should be noted that many experimental investigations of optical forces are done with particles, dissolved in liquid solutions. In such environments, optically denser particles can be used in order to achieve sufficient force amplitude, see the Supporting Information, F.

To get a deeper insight into the differences between homogenized and layered cases, the imaginary part of the reflection coefficient was plotted, as the function of the transversal component of the wave vector of incident wave, Figure 4b. Metal-dielectric stacks with different periodicity, but with the same filling factors (homogenized parameters are supposed to be the same), were investigated. Multilayer substrates feature strongly nonuniform dependence of Im-$(r_p(k_\rho))$. The lowest reflectivity of evanescent waves is obtained in the case, where the top layer is the dielectric. As a result, the lowest pulling force values are obtained (see panel (a)). As metal layer is placed on the top, situation changes drastically. Sharp peak in r_p at k_ρ slightly exceeding k_1 is linked with the existence of the long-range plasmon (LR-SPP). Furthermore, at $k_\rho \gg k_1$ reflection coefficient obtains significant values in the allowed zone of the periodic structure. Here the reflection coefficient exceeds r_p^∞ (characteristic to homogeneous hyperbolic material at large k_ρ) due to the short-range plasmon (SR-SPP).[40] Convolution of such $r_p(k_\rho)$, enhanced by short-range plasmon, with an exponentially decaying term in the integrand of eq 4 defines features, characteristic to different periods of the unit cell.

Concluding this part of the investigation, both volume modes and SR-SPP, linked with $\mathrm{Im}(r_p(k_\rho))$, are crucial for optical forces. Increasing $\mathrm{Im}(r_p(k_\rho))$ at the region of evanescent waves can lead to the enhancement of the puling force. As for SPP resonance at the bulk metal interface, considered previously in ref 21, it is also characterized by $\mathrm{Im}(r_p(k_\rho))$ increase for a broad range of evanescent k_ρ. However, in this case, the effect is associated with a sharp spectral resonance (plasmonic branch). For low-loss metals, it results in strong pulling forces, for example, for Ag substrate tractor beam takes place at wavelength around 340 nm, corresponding to SPP resonance. Besides narrow-band spectral dependence, the amplitude of pulling force will drop significantly with an increase of absorption in metal, what complicates the experimental applications of SPP resonance-assisted tractor beam in the visible range. Note that different physical trends are expected for optical forces due to different kind of modes at the substrate interface and within the bulk. In particular, spectral features and loss dependence of volumetric modes can be tailored and subsequently employed for achieving significant values of pulling forces.

While the beforehand studies of the forces were performed on the configurations, where the metal was chosen to be silver, other plasmonic materials are of a potential interest (especially with the development of other promising alternatives[44]). Hereafter, Au (3−5 nm) and Ag (1.5−3 nm) thick layers will be compared with each other and with semi-infinite substrates, made of a solid metal (traditional plasmonic substrate). Figure 5 summarizes the results. The pulling force at pure metal substrate emerges solely owing to the interaction with surface plasmon polaritons at the resonance. Bulk silver, having smaller optical losses than gold, provides very strong optical force, while gold substrate gives very low force amplitude. Single isolated Ag layer can also provide a pulling force due to SR-SPP, however, this effect is relatively weak and is not presented here. For both Au and Ag multilayers the force spectra are red-shifted with respect to the bulk substrates. In addition, the force bandwidths are significantly wider for the layers. Remarkably, in the multilayer hyperbolic case, pulling forces are much stronger than for a bulk Au substrate and less affected by material loss−both gold and silver layers show

DOI: 10.1021/acsphotonics.8b00775
ACS Photonics 2018, 5, 4371−4377

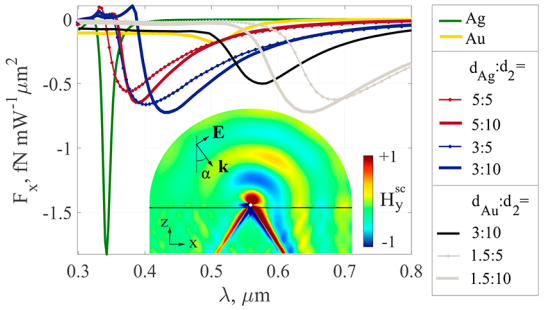

Figure 5. Transversal force F_x acting on a particle (R = 15 nm, ε = 3, z = 15 nm) for different types of substrates: silver (green line), gold (yellow line), Ag-polymer multilayer (red and blue lines), and Au-polymer multilayer (black and gray lines). In legend d_{Ag}, d_{Au}, d_2 are specified in nm and stand for Ag, Au, and polymer thicknesses. Multilayer is terminated with metal; plane wave is incident at 35°. The inset shows magnetic component H_y^{sc} of the field scattered by the particle above the homogeneous hyperbolic substrate (for the effective model of Ag-polymer multilayer f_{Ag} = 0.2 at λ = 450 nm), z = 16 nm, α = 35°.

similar amplitudes. Broadband force enhancement is achieved with multilayer substrates in the whole visible range from 400 to 800 nm. Unlike purely plasmonic case, hyperbolic modes are less affected by losses. It is worth noting that virtually any metal provides noticeable negative force (Supporting Information, E) and is suitable for optomechanical applications.

Inset in Figure 5 shows a FEM simulation of magnetic field scattered by a particle (excluding background field given by the incident and reflected plane waves) for the homogeneous hyperbolic material. Highly confined high-k volume modes are seen in the substrate and are typical to hyperbolic metamaterial (e.g., see ref 45). The asymmetric scattering pattern within the substrate visualizes the puling force effect and the impact of the metamaterial. The substrate opens the high DOS channels and allows tailoring forces by breaking the symmetry of the momentum, carried out by the scattered waves. Furthermore, high-k waves carry more momentum in comparison to free space counterparts and, as the result, recoil force values increase.

Summarizing, multilayered metamaterials can be used as effective substrates for achieving negative optical forces, which, compared to the plasmonic substrates, provide a set of new features: (1) broadband pulling force (instead of narrowband response at the surface plasmon resonance or a weak response at SR-SPP), (2) tuning the position of the force spectra by appropriate design of the multilayer structure, and (3) large negative force for multilayers with lossy metals.

CONCLUSIONS

Optical forces mediated by hyperbolic metamaterials interfacing dielectric homogeneous space (e.g., air or water, in the case of fluidic applications) were theoretically investigated. Strong optical pulling forces were obtained over the broad spectral range and this new effect is attributed to the hyperbolic type of dispersion of electromagnetic modes. Analytical formalism of the phenomenon was developed and it relies on the self-consistent expressions for the total field at the particle location, given with the help of electromagnetic Green's function. Spectral decomposition of the Green's function enabled identifying contributions of different interaction channels into the total optical force. In particular, long-range surface plasmon polaritons having sharp resonance in k-space were separated from the hyperbolic bulk modes for the case of homogeneous hyperbolic material. Hyperbolic modes, having high density of electromagnetic states over a broad spectral range, are the preferable channel for scattering. It was shown that the hyperbolicity of the substrate plays the key role in delivering the overall effect in the broad spectral range. However, multilayered realization of the metamaterial, when the top material interfacing the air is metal, introduces an important contribution to the value of the pulling force. The broadband property and tunability of the hyperbolic metasurface have an additional key advantage over a single metal layer—optical attraction can be achieved at the infrared spectral range, which is highly important to many optomechanical applications. Metasurfaces, designed to control near-field interactions, open a venue for flexible optomechanical manipulation schemes. While the effect of optical attraction was demonstrated here, other important fundamental phenomena and applications, such as optical binding, sorting, trapping, to name just few, can be enabled by carefully designed optomechanical metasurfaces.

ASSOCIATED CONTENT

Supporting Information

The Supporting Information is available free of charge on the ACS Publications website at DOI: 10.1021/acsphotonics.8b00775.

A, Literature review; B, Force calculation formalism; C, Green's function and excitation conditions; D, Applicability of effective medium theory to optical forces calculations; E, Optimization of multilayers for negative optical force; F, Particles suspended in water (PDF).

AUTHOR INFORMATION

Corresponding Author

*E-mail: ivinskaya@tut.by.

ORCID

Aliaksandra Ivinskaya: 0000-0002-0262-6459
Mihail I. Petrov: 0000-0001-8155-9778
Andrey A. Bogdanov: 0000-0002-8215-0445
Alina Karabchevsky: 0000-0002-4338-349X

Author Contributions

A.I. designed the model and the computational framework and analyzed the data. A.I. and P.G. wrote the manuscript. A.A.B. and A.P. performed finite element simulations. P.G. and A.S.S. supervised the work. All authors contributed to the research activities.

Funding

The authors gratefully acknowledge the financial support provided by Russian Foundation for Basic Research (Project Nos. 18-02-00414 and 18-52-00005); Ministry of Education and Science of the Russian Federation (Grants No. 3.4982.2017/6.7 and No. 3.1668.2017/4.6); The force calculations were partially supported by Russian Science Foundation (Grant No. 18-72-10127). A.K. acknowledges the support of the Israeli Ministry of Trade and Labor-Kamin Program, Grant. No. 62045. A.B. acknowledges the support of the Russian Fundation for Basic Research (16-37-60064). P.G. acknowledges PAZY Foundation (Grant No. 01021248) and ERC StG 'In Motion'.

DOI: 10.1021/acsphotonics.8b00775
ACS Photonics 2018, 5, 4371−4377

Notes

The authors declare no competing financial interest.

REFERENCES

(1) Ashkin, A. Acceleration and Trapping of Particles by Radiation Pressure. *Phys. Rev. Lett.* **1970**, *24*, 156−159.
(2) Neuman, K. C.; Block, S. M. Optical Trapping. *Rev. Sci. Instrum.* **2004**, *75*, 2787−2809.
(3) Grier, D. G. A Revolution in Optical Manipulation. *Nature* **2003**, *424*, 810−816.
(4) Svoboda, K.; Block, S. M. Biological Applications of Optical Forces. *Annu. Rev. Biophys. Biomol. Struct.* **1994**, *23*, 247−285.
(5) Jagannathan, B.; Marqusee, S. Protein Folding and Unfolding under Force. *Biopolymers* **2013**, *99*, 860−869.
(6) Padgett, M.; Di Leonardo, R. Holographic Optical Tweezers and Their Relevance to Lab on Chip Devices. *Lab Chip* **2011**, *11*, 1196−1205.
(7) Singh, B. K.; Nagar, H.; Roichman, Y.; Arie, A. Particle Manipulation beyond the Diffraction Limit Using Structured Super-Oscillating Light Beams. *Light: Sci. Appl.* **2017**, *6*, e17050.
(8) Juan, M. L.; Righini, M.; Quidant, R. Plasmon Nano-Optical Tweezers. *Nat. Photonics* **2011**, *5*, 349−356.
(9) Gu, M.; Bao, H.; Gan, X.; Stokes, N.; Wu, J. Tweezing and Manipulating Micro- and Nanoparticles by Optical Nonlinear Endoscopy. *Light: Sci. Appl.* **2014**, *3*, e126.
(10) Okamoto, K.; Kawata, S. Radiation Force Exerted on Subwavelength Particles near a Nanoaperture. *Phys. Rev. Lett.* **1999**, *83*, 4534−4537.
(11) Yan, Z.; Bao, Y.; Manna, U.; Shah, R. A.; Scherer, N. F. Enhancing Nanoparticle Electrodynamics with Gold Nanoplate Mirrors. *Nano Lett.* **2014**, *14*, 2436−2442.
(12) Lin, P.-T.; Chu, H.-Y.; Lu, T.-W.; Lee, P.-T. Trapping Particles Using Waveguide-Coupled Gold Bowtie Plasmonic Tweezers. *Lab Chip* **2014**, *14*, 4647−4652.
(13) Conteduca, D.; Reardon, C.; Scullion, M. G.; Dell'Olio, F.; Armenise, M. N.; Krauss, T. F.; Ciminelli, C. Ultra-High Q/V Hybrid Cavity for Strong Light-Matter Interaction. *APL Photonics* **2017**, *2*, 086101.
(14) Markovich, H.; Shishkin, I.; Hendler, N.; Ginzburg, P. Optical Manipulation along Optical Axis with Polarization Sensitive Meta-Lens. *Nano Lett.* **2018**, *18*, 5024−5029.
(15) Volpe, G.; Quidant, R.; Badenes, G.; Petrov, D. Surface Plasmon Radiation Forces. *Phys. Rev. Lett.* **2006**, *96*, 238101.
(16) Shilkin, D. A.; Lyubin, E. V.; Soboleva, I. V.; Fedyanin, A. A. Trap Position Control in the Vicinity of Reflecting Surfaces in Optical Tweezers. *JETP Lett.* **2014**, *98*, 644−647.
(17) Novitsky, A.; Qiu, C.; Wang, H. Single Gradientless Light Beam Drags Particles as Tractor Beams. *Phys. Rev. Lett.* **2011**, *107*, 203601.
(18) Sukhov, S.; Dogariu, A. Negative Nonconservative Forces: Optical 'Tractor Beams' for Arbitrary Objects. *Phys. Rev. Lett.* **2011**, *107*, 203602.
(19) Chen, J.; Ng, J.; Lin, Z.; Chan, C. T. Optical Pulling Force. *Nat. Photonics* **2011**, *5*, 531−534.
(20) Kajorndejnukul, V.; Ding, W.; Sukhov, S.; Qiu, C.-W.; Dogariu, A. Linear Momentum Increase and Negative Optical Forces at Dielectric Interface. *Nat. Photonics* **2013**, *7*, 787−790.
(21) Petrov, M. I.; Sukhov, S. V.; Bogdanov, A. A.; Shalin, A. S.; Dogariu, A. Surface Plasmon Polariton Assisted Optical Pulling Force. *Laser Photon. Rev.* **2016**, *10*, 116−122.
(22) Shilkin, D. A.; Lyubin, E. V.; Soboleva, I. V.; Fedyanin, A. A. Direct Measurements of Forces Induced by Bloch Surface Waves in a One-Dimensional Photonic Crystal. *Opt. Lett.* **2015**, *40*, 4883−4886.
(23) Shilkin, D. A.; Lyubin, E. V.; Soboleva, I. V.; Fedyanin, A. A. Near-Field Probing of Bloch Surface Waves in a Dielectric Multilayer Using Photonic Force Microscopy. *J. Opt. Soc. Am. B* **2016**, *33*, 1120−1127.
(24) Cai, W.; Shalaev, V. *Optical Metamaterials - Fundamentals and Applications*; Springer-Verlag: New York, 2010.
(25) Jacob, Z.; Smolyaninov, I. I.; Narimanov, E. E. Broadband Purcell Effect: Radiative Decay Engineering with Metamaterials. *Appl. Phys. Lett.* **2012**, *100*, 181105.
(26) Bogdanov, A. A.; Shalin, A. S.; Ginzburg, P. Optical Forces in Nanorod Metamaterial. *Sci. Rep.* **2015**, *5*, 15846.
(27) Shalin, A. S.; Sukhov, S. V.; Bogdanov, A. A.; Belov, P. A.; Ginzburg, P. Optical Pulling Forces in Hyperbolic Metamaterials. *Phys. Rev. A: At., Mol., Opt. Phys.* **2015**, *91*, 063830.
(28) Yu, N.; Capasso, F. Flat Optics with Designer Metasurfaces. *Nat. Mater.* **2014**, *13*, 139−150.
(29) Shitrit, N.; Yulevich, I.; Maguid, E.; Ozeri, D.; Veksler, D.; Kleiner, V.; Hasman, E. Spin-Optical Metamaterial Route to Spin-Controlled Photonics. *Science* **2013**, *340*, 724−726.
(30) Kildishev, A. V.; Boltasseva, A.; Shalaev, V. M. Planar Photonics with Metasurfaces. *Science* **2013**, *339*, 1232009.
(31) Yermakov, O. Y.; Ovcharenko, A. I.; Song, M.; Bogdanov, A. A.; Iorsh, I. V.; Kivshar, Y. S. Hybrid Waves Localized at Hyperbolic Metasurfaces. *Phys. Rev. B: Condens. Matter Mater. Phys.* **2015**, *91*, 235423.
(32) High, A. A.; Devlin, R. C.; Dibos, A.; Polking, M.; Wild, D. S.; Perczel, J.; De Leon, N. P.; Lukin, M. D.; Park, H. Visible-Frequency Hyperbolic Metasurface. *Nature* **2015**, *522*, 192−196.
(33) Chaumet, P. C.; Nieto-Vesperinas, M. Time-Averaged Total Force on a Dipolar Sphere in an Electromagnetic Field. *Opt. Lett.* **2000**, *25*, 1065−1067.
(34) Novotny, L.; Hecht, B. *Principles of Nano-Optics*, 2nd ed.; Cambridge University Press, 2012.
(35) Zhukovsky, S. V.; Andryieuski, A.; Takayama, O.; Shkondin, E.; Malureanu, R.; Jensen, F.; Lavrinenko, A. V. Experimental Demonstration of Effective Medium Approximation Breakdown in Deeply Subwavelength All-Dielectric Multilayers. *Phys. Rev. Lett.* **2015**, *115*, 177402.
(36) Krishnamoorthy, H. N. S.; Jacob, Z.; Narimanov, E.; Kretzschmar, I.; Menon, V. M. Topological Transitions in Metamaterials. *Science* **2012**, *336*, 205−209.
(37) West, P. R.; Ishii, S.; Naik, G.; Emani, N.; Shalaev, V. M.; Boltasseva, A. Searching for Better Plasmonic Materials. *Light Sci. Appl.* **2010**, *4*, 795−808.
(38) Saarinen, J. J.; Sipe, J. E. A Green Function Approach to Surface Optics in Anisotropic Media. *J. Mod. Opt.* **2008**, *55*, 13−32.
(39) Iorsh, I.; Orlov, A.; Belov, P.; Kivshar, Y. Interface Modes in Nanostructured Metal-Dielectric Metamaterials. *Appl. Phys. Lett.* **2011**, *99*, 151914.
(40) Kidwai, O.; Zhukovsky, S. V.; Sipe, J. E. Effective-Medium Approach to Planar Multilayer Hyperbolic Metamaterials: Strengths and Limitations. *Phys. Rev. A: At., Mol., Opt. Phys.* **2012**, *85*, 053842.
(41) Chebykin, A. V.; Orlov, A. A.; Simovski, C. R.; Belov, P. A. Nonlocal Effective Parameters of Multilayered Metal-Dielectric Metamaterials. *Phys. Rev. B: Condens. Matter Mater. Phys.* **2012**, *86*, 115420.
(42) Chebykin, A. V.; Babicheva, V. E.; Iorsh, I. V.; Orlov, A. A.; Belov, P. A.; Zhukovsky, S. V. Enhancement of the Purcell Factor in Multiperiodic Hyperboliclike Metamaterials. *Phys. Rev. A: At., Mol., Opt. Phys.* **2016**, *93*, 033855.
(43) Rodríguez-Fortuño, F. J.; Zayats, A. V. Repulsion of Polarised Particles from Anisotropic Materials with a Near-Zero Permittivity Component. *Light: Sci. Appl.* **2016**, *5*, e16022.
(44) Naik, G. V.; Shalaev, V. M.; Boltasseva, A. Alternative Plasmonic Materials: Beyond Gold and Silver. *Adv. Mater.* **2013**, *25*, 3264−3294.
(45) Ginzburg, P.; Krasavin, A. V.; Poddubny, A. N.; Belov, P. A.; Kivshar, Y. S.; Zayats, A. V. Self-Induced Torque in Hyperbolic Metamaterials. *Phys. Rev. Lett.* **2013**, *111*, 036804.

DOI: 10.1021/acsphotonics.8b00775
ACS Photonics 2018, 5, 4371−4377